Journal of Solid State Chemistry **147,** 328–335 (1999)
Article ID jssc.1999.8301, available online at http://www.idealibrary.com on IDEAL®

Heterostructured Bi-Based Cuprate High-T_c Superconductors with Unusually Coordinated Metal Halides

J.-H. Choy,*,[1] Y.-I. Kim,* S.-J. Hwang,* and I.-S. Yang†

*Department of Chemistry, Center for Molecular Catalysis, College of Natural Sciences, Seoul National University, Seoul 151-742, Korea; and †Department of Physics, Ewha Womans University, Seoul 120-750, Korea

Received December 18, 1998; in revised from March 19, 1999; accepted March 23, 1999

Attempts have been made to prepare various high-T_c superconducting intercalation compounds, M–X–$Bi_2Sr_2Ca_{n-1}Cu_nO_{2n+4+\delta}$ (M=metal; X=halogen; $n=1$, 2, and 3), with the synthetic strategy of hard–soft–acid–base interaction. The *chimie douce* route such as vapor transport and ionic diffusion is found to be effective in intercalating soft Lewis acidic guest species (I_3^-, $Ag_xI_w^{x-w}$, $HgI_2^{\delta-}$, $HgBr_2^{\delta-}$, and $AuI_3^{\delta-}$) into the Lewis basic $Bi_2Sr_2Ca_{n-1}Cu_nO_{2n+4+\delta}$ lattice. According to the X-ray diffraction and magnetic property measurements on these intercalates, it becomes clear that the basal increment upon intercalation (3.25–7.35 Å) is governed by the interlayer geometry of the intercalant, while the accompanying T_c change depends on the charge transfer between host and guest. The extended X-ray absorption fine structure and Raman studies reveal that mercuric halides are intercalated as linear molecules as in vapor state, while silver iodide forms a two-dimensionally extended ionic-conducting channel. In the case of new gold iodide intercalate, unique trigonal planar AuI_3 species is identified as the first example of an isolated gold iodide molecule. © 1999 Academic Press

INTRODUCTION

The intercalation into high-T_c superconducting Bi-based cuprates, $Bi_2Sr_2Ca_{n-1}Cu_nO_{2n+4+\delta}$ ($n=1$, 2, and 3), has attracted intense research interest since it can provide a unique chemical way to hybridize superconducting lattice with a two-dimensional array of foreign atoms, molecules, or ions (1–26). In 1990, it was first reported that iodine can be intercalated into the Bi-based cuprate, $Bi_2Sr_2CaCu_2O_{8+\delta}$ (2), which became a good model compound not only to rationalize the superconductivity behavior of slightly perturbed system but also to develop new intercalation derivatives of Bi-based cuprates. The iodine molecule, classified into a soft acid group based on the hard–soft–acid–base (HSAB) concept, is known to be stabilized as the triiodide (I_3^-) ion in the interlayer space of Bi_2O_2 double layer of $Bi_2Sr_2CaCu_2O_{8+\delta}$ (3, 4), since the superconducting host lattice, which can be considered a large molecular cluster if it is separated by a large guest, behaves as a soft base with electron-donating character. It is therefore speculated that the soft–soft interaction is an important factor in realizing intercalation reaction into Bi-based cuprate, which was further supported by the unsuccessful results to intercalate hard acids or hard bases such as Li, Na, K, Cu, Ag, $FeCl_3$, $AlCl_3$, pyridine, alkylamine, and ammonium salt (5, 6).

In addition to such a thermodynamic aspect based on the HSAB interaction (27), the intercalation kinetics should be taken into account in selecting the possible intercalants. Considering the chemical stability of the host lattice, it is quite desirable to react at relatively low temperature (below 300°C) without strong acidic or basic medium. It is therefore necessary to find intercalant that is highly mobile enough to diffuse into the host lattice under such a mild condition. In this context, the criteria for possible intercalant can be established as follows: (i) The polarizability of intercalant must be high, since it is directly related to its softness, that is, to the deformability of its electron cloud. Thus, large and highly charged intercalants are especially prone to polarization and covalent character eventually leading to intercalation. (ii) Intercalant must be highly mobile at relatively low temperature and at the same time chemically inert to the host oxide lattice. Among various metal salts and molecular compounds we were able to find several intercalants that satisfy the above criteria, and eventually we were able to explore chemically and structurally well-defined intercalated bismuth cuprate systems hybridized with intercalants such as iodine, mercuric bromide, mercuric iodide, silver iodide, and gold iodide (7–16).

Previously we have investigated the intracrystalline structure of mercuric halides and silver iodide intercalated in the Bi-based cuprate (12, 13). For both cases, it was found that the intercalated metal halides exist as their high temperature forms even at room temperature, which might be indispensable for the respective intercalation conditions. The only

[1] To whom correspondence should be addressed. Fax: (82)2-872-9864. E-mail: jhchoy@snu.ac.kr.

0022-4596/99 $30.00

possible meaning such high temperature states can have is to indicate that if a salt molecule stabilized in the Bi-based cuprate could exist, it should accept electrons from the host lattice, that is, from CuO_2 layers as observed in the iodine intercalate immediately to form $HgX_2^{-\delta}$ and $AgI^{-\delta}$ in such a way that it can be easily polarized to form a bond with the host. In the context, it must be quite interesting to elucidate the geometric structure of intercalated Au–I species, since Au–I intercalation is performed at a temperature (235°C) much higher than the decomposition temperature of AuI (100°C) (28). In this paper, we present the various examples of recently developed superconducting intercalation compounds. The combinative extended X-ray absorption fine structure (EXAFS) and Raman analyses have been performed to determine the intracrystalline structure of intercalated HgI_2, $HgBr_2$, Ag–I, and Au–I species.

EXPERIMENTAL

Synthesis

The pristine $Bi_2Sr_2Ca_{n-1}Cu_nO_{2n+4+\delta}$ ($n = 1$, 2, and 3) compounds were prepared by conventional solid state reaction as reported previously (29). The single-phase intercalates of iodine and mercuric halides were obtained by heating the pristine polycrystals with $\sim$5 mole excess of guest molecules in an evacuated Pyrex tube at 180°C for iodine and at 230–240°C for HgX_2 (X = Br and I). In the case of HgI_2 intercalate, one equivalent mole of I_2 is also required as a transporting reagent for completing the intercalation reaction. On the other hand, the intercalation of silver iodide and gold iodide could be achieved through the liquid-like mobilities of Ag^+ and Au^+ within the iodide lattice. Since both iodides, AgI (30) and AuI (31), are known to be unusually fast ionic-conducting, we have designed a reaction scheme where the cation migrates into the interlayer iodide region of iodine-intercalated bismuth cuprate from the host lattice boundary. The Ag–I intercalate was prepared by heating the mixture of AgI and iodine intercalate at 190°C for 10 h in air, where the stoichiometry of intercalant layer could be modified by changing the mixing ratio of AgI and iodine intercalate. Similarly, Au–I intercalation was accomplished by heating a mixture of iodine intercalate and 0.25 equimolar Au at 235°C for 8 h in an ambient atmosphere. For all the present metal salt intercalates, no spontaneous disintercalation was observed in an ambient condition, indicating that the intercalant metal salts can form the stable intercalation complexes with Bi-based cuprates. Such a chemical stability of these intercalates was further evidenced by the X-ray diffraction (XRD) and EXAFS measurements for the samples stored for several months where their crystal structure and electronic configuration are found to remain the same as those of as-prepared samples.

Characterizations

The powder XRD pattern was measured using a Phillips PW 3710 powder diffractometer equipped with Ni-filtered Cu$K\alpha$ radiation ($\lambda = 1.5405$ Å), operated at 20 mA and 40 kV. The chemical compositions of all the intercalates were determined by using electron microprobe analysis (EPMA), thermogravimetry (TG), or X-ray photoelectron spectroscopy (XPS). The electronic and geometric structures of intercalants were investigated by performing X-ray absorption measurements at the beam lines 10B and 7C in Photon Factory (Tsukuba) operated at 2.5 GeV and 300–360 mA. The Raman measurements were carried out at room temperature using a Jobin-Yvon U1000 spectrometer with Olympus metallurgical microscope and/or a Jobin-Yvon/Atago Bussan T64000 triple spectrometer equipped with microoptics. The samples were excited with the 514.5-nm line of Ar^+ laser. The T_c evolution upon intercalation was examined by performing dc magnetic susceptibility and four-probe resistivity measurements. Ionic conductivity of Ag–I intercalates was measured by impedance spectroscopy using an electron-blocking cell $Ag/AgI/(Ag_xI_w)Bi_2Sr_2Ca_{n-1}Cu_nO_{2n-4+\delta}/AgI/Ag$ in order to separate the partial ionic contribution in a mixed ionic–electronic conductor.

DATA AND DISCUSSION

HgX_2 Intercalates (X = Br and I)

Due to the high volatility of mercuric halides, the HgX_2 intercalates can be synthesized easily by the vapor transport reaction between HgX_2 and the pristine compound. According to the XRD analysis of these mercuric halide derivatives, the c-axial lattice expansions (Δd) are estimated to be $\sim$6.3 Å for the $HgBr_2$ intercalate and $\sim$7.2 Å for the HgI_2 one, values almost twice as large as that for the iodine intercalate. Such basal increments indicate that the halogen bilayers are formed in the interlayer space of metal halide intercalates.

From the magnetic susceptibility measurements, both HgX_2 intercalates are found to exhibit bulk superconductivity with a slight T_c decrease of 5–8 K, compared to the pristine compound. It is worthwhile to note here that the T_c depression upon HgX_2 intercalation is smaller than that upon iodine intercalation, despite larger lattice expansion for the former, due to the fact that interlayer coupling is not a main factor for superconductivity.

Concerning the intracrystalline structure of mercuric halides intercalated in Bi-based cuprates, the previous Hg L_3-edge EXAFS studies on these intercalates indicated that the intercalated mercuric halide is stabilized as a linear molecule as in a vapor state (12). However, the severe dynamic disorder prevents probing of distant coordination shells around mercury by room temperature EXAFS analysis, and therefore the Hg local symmetry of $HgBr_2$ intercalate was

not clearly differentiated from that of $HgBr_2$ solid. That is, according to the previous EXAFS results, the coordination number of mercury was determined to be 2 not only for the $HgBr_2$ intercalate but also for free $HgBr_2$, which is surely incomparable with the crystallographic data (31). In order to solve such a problem, we have carried out the low-temperature EXAFS experiment on these compounds, because the lowering of measurement temperature leads to the suppression of thermal disorder (33).

The temperature-dependent Hg L_3-edge EXAFS spectra for the $HgBr_2$ intercalate and the unintercalated $HgBr_2$ solid are shown in Fig. 1a, and the corresponding Fourier transforms (FTs) in Fig. 1b. In contrast to the $HgBr_2$ intercalate, there are remarkable changes in the FT of $HgBr_2$, depending upon the measurement temperature. While only a single peak is observed at about 2.1 Å in the spectrum measured at 300 K, two peaks are detected around 2.1 and 2.9 Å in the spectrum measured at 20 K. These coordination shells corresponding to (Hg–Br) bonding pairs were isolated by inverse Fourier transformation to k space as shown in Fig. 2, and the curve fittings were carried out to them to determine the structural parameters such as coordination number (CN), bond length (R), and Debye–Waller factor (σ^2). The amplitude of EXAFS oscillation is found to increase remarkably for the 20 K spectrum of $HgBr_2$ with respect to the corresponding 300 K one, whereas there is only a negligible amplitude difference in both present spectra of $HgBr_2$ intercalate. Generally the amplitude in k space is mainly affected by the following two factors: one is the effect of neighboring atoms, which means that the signal tends to enhance as the coordination number increases, and the other is the effect of the Debye–Waller factor, whose increase gives rise to a depression of EXAFS oscillation (34). It has been also well known that the Debye–Waller factor is dependent upon two kinds of structural deformation, ie., temperature-dependent thermal disorder and temperature-independent static one (34). In this respect, the prominent amplitude enhancement for $HgBr_2$ induced by lowering of temperature accounts for a decrease in thermal disorder. It is also observed that the 20 K spectrum of free $HgBr_2$ shows the dissimilar oscillation frequency from the corresponding 300 K one, whereas there is an insignificant frequency difference between both present spectra of $HgBr_2$ intercalate. Moreover,the low-temperature EXAFS spectrum of $HgBr_2$ has two nodes in the present k range, implying the existence of more than two shells, which is consistent with the observed two peaks in the corresponding FT. The best fitting results to these coordination shells are compared to the experimental spectra in Figs. 1b and 2, and the fitted structural parameters are summarized in Table 1. Since the

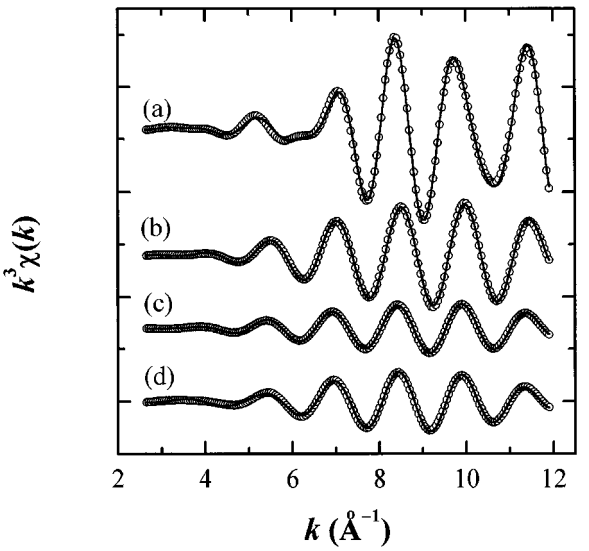

FIG. 2. Comparison of the fitted Hg L_3-edge EXAFS spectra with the experimental data of $HgBr_2$ at (a) 20 K and (b) 300 K and $(HgBr_2)_{0.5}Bi_2Sr_2CaCu_2O_{8+\delta}$ at (c) 20 K and (d) 300 K (experimental, open circle; fit, solid line).

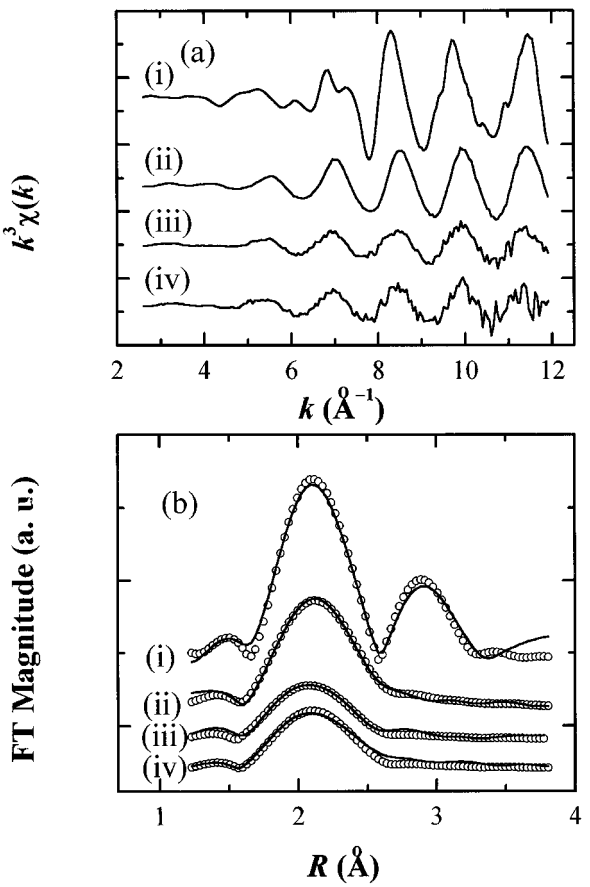

FIG. 1. (a) Experimental k^3-weighted Hg L_3-edge EXAFS spectra and (b) their Fourier transforms of $HgBr_2$ at (i) 20 K and (ii) 300 K and $(HgBr_2)_{0.5}Bi_2Sr_2CaCu_2O_{8+\delta}$ at (iii) 20 K and (iv) 300 K (experimental, open circle; fit, solid line).

coordination number obtained from the fitting analysis corresponds to the product of coordination number and the amplitude reduction factor (S_0^2), it is necessary to get the amplitude reduction factor for a specific absorber–scatterer pair prior to determining the exact coordination number (34). In the present analysis, the amplitude reduction factors obtained from the free $HgBr_2$ reference (0.82_3 and 0.80_3 for 20 and 300 K, respectively) were used to calculate the coordination number of mercury in the $HgBr_2$ intercalate. As listed in Table 1, the intercalated mercuric bromide has a linear two-coordinated structure even at 20 K, as in the case of $HgBr_2$ vapor (32, 35). On the contrary, the fitting analysis to the 20 K spectrum of $HgBr_2$ solid clarifies that this compound has a $HgBr_6$ octahedron with $R_{Hg-Br} = 2.46$ Å ($\times 2$) for the first shell and 3.20 Å ($\times 4$) for the second one, which is consistent with the previous crystallographic study (32). Such crystal structure data are quite different from those determined from the corresponding 300 K spectrum. This is surely attributed to a severe thermal disorder at room temperature, reducing the peak amplitude in FT (34). From the above experimental findings, it becomes clear that the intercalated mercuric bromide has a molecule-like intracrystalline structure, which is surely distinguished from the CdI_2-type structure of unintercalated $HgBr_2$ solid.

Further evidence on the linear HgX_2 molecule in between Bi_2O_2 layers can be obtained from micro-Raman studies. As shown in Fig. 3, both Raman spectra of HgX_2 intercalates exhibit a characteristic peak corresponding to the symmetric stretching (v_1) vibration of (Hg–X) at around 170 cm^{-1} for the $HgBr_2$ intercalate and 130 cm^{-1} for the HgI_2 one, confirming the linear local structure of intercalated mercuric halides. Based on the present spectroscopic evidences on the linear HgX_2 molecule, one-dimensional electron density maps along the c axis of intercalates have been calculated, revealing that the $HgBr_2$ molecular axis for instance is tilted at an angle of 65° with respect to the c axis. Such a tilted configuration would be advantageous to get the stabilization energy through the van der Waals interaction with adjacent guest molecules.

TABLE 1
Results of Nonlinear Least-Square Curve Fitting for the Hg L_3-Edge EXAFS Spectra

Compound	R (Å)	CN	σ^2 (10^{-3} Å^2)
$HgBr_2$ (300 K)	2.45_9	2[a]	3.09
$HgBr_2$ (20 K)	2.45_6	2[a]	1.57
	3.20_0	4[a]	6.67
$(HgBr_2)_{0.5}Bi_2Sr_2CaCu_2O_{8+\delta}$ (300 K)	2.46_2	1.85_7	6.41
$(HgBr_2)_{0.5}Bi_2Sr_2CaCu_2O_{8+\delta}$ (20 K)	2.45_4	1.70_1	6.30

[a] The coordination number (CN) of reference $HgBr_2$ was fixed to the crystallographic value with a view to determining the amplitude reduction factor (S_0^2).

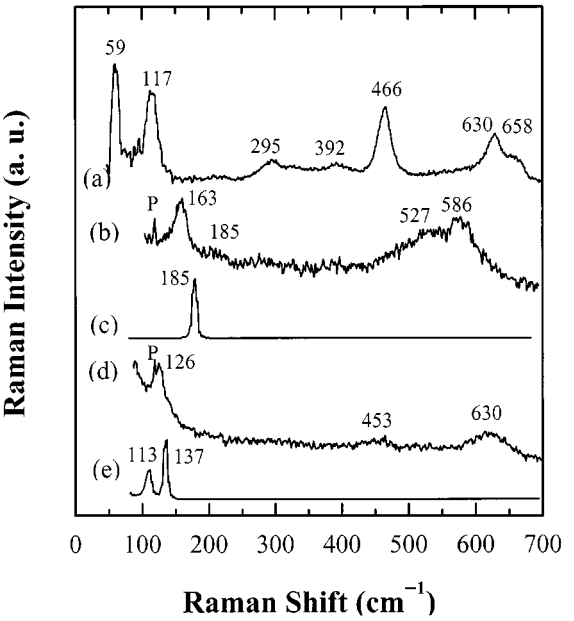

FIG. 3. Micro-Raman spectra of (a) the pristine $Bi_2Sr_2CaCu_2O_{8+\delta}$ and its HgX_2 intercalates with (b) X = Br and (d) X = I, together with the references of (c) $HgBr_2$ and (e) red HgI_2. The symbol P indicates the Ar plasma line of the laser beam.

Ag_xI_w Intercalate

As mentioned above, Ag–I intercalation into Bi-based cuprates is accomplished in two steps: (i) iodine intercalation and (ii) Ag^+ ionic diffusion into the intercalated iodide sublattice. During the second step, the interlayer iodines are also thermally activated and rearranged to coordinate effectively to the Ag ion. Such a structural transformation of the Ag–I lattice is propagated by gradual Ag insertion.

The intracrystalline structure of the Ag–I sublattice has been probed by EXAFS analysis. From the nonlinear curve fitting to the Fourier-filtered EXAFS spectra at the Ag K- and I L_3-edges, it is found that the AgI_4 tetrahedra are stabilized in the interlayer space of the host lattice. Since the lattice expansion of Ag–I intercalate ($\Delta d \approx 7.3$ Å) is approximately twice as large as that of the iodine one ($\Delta d \approx 3.6$ Å), the interlayer Ag–I lattice can be described as the monolayered network of edge-shared AgI_4 tetrahedra (Fig. 4). Moreover, it is also revealed that, in the Ag–I intercalates with a larger Ag content, the Coulombic Ag^+–Ag^+ repulsion may give rise to a slight displacement of Ag from the center of the AgI_4 tetrahedron.

Such a structural disorder around the interlayer Ag ion has also been examined by performing Raman measurements. Figure 5 represents the unpolarized Raman spectra of $Bi_2Sr_2CaCu_2O_{8+\delta}$ and $Ag_xI_wBi_2Sr_2CaCu_2O_{8+\delta}$ (x = 0.76, 1.0, and 1.17), in comparison with those of the references α-AgI (at 160°C) and β-AgI (at 20°C). The pristine

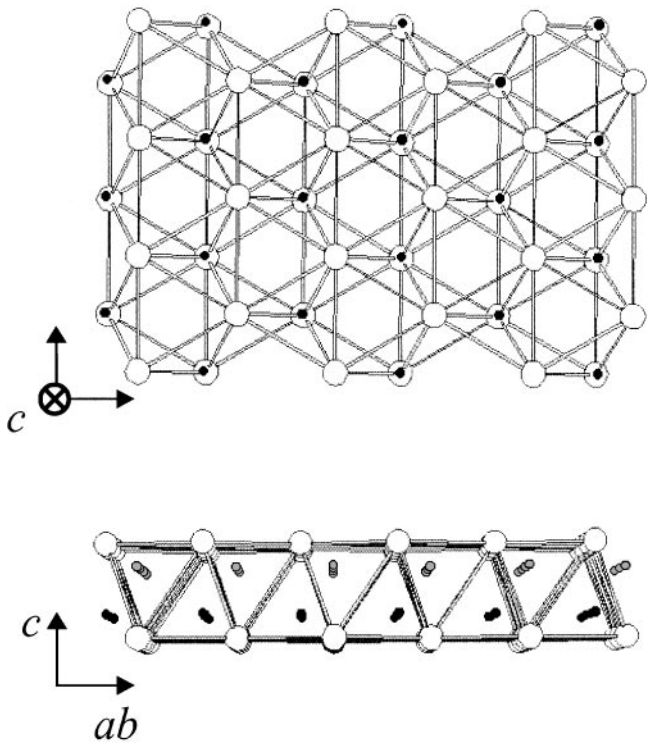

FIG. 4. Two-dimensionally expanded Ag–I lattice, which is formed by the edge-sharing between the AgI_4 tetrahedra.

$Bi_2Sr_2CaCu_2O_{8+\delta}$ compound exhibits Raman spectral features corresponding to the tetragonal structure with the space group $I4/mmm$ (36). However, such phonon modes of the host lattice are significantly suppressed upon Ag–I intercalation, due to the much stronger Raman activity of the guest Ag–I layer. In the case of α- and β-AgI spectra (37), there are significant changes caused by structural transition at 147°C. Since AgI has the β-type wurtzite structure below this transition temperature (32), the peaks at 17, 106, and 124 cm^{-1} in β-AgI are attributed to the E_2, $A_1(TO)/E_1(TO)$, and $A_1(LO)/E_1(LO)$ modes, respectively (38, 39). The residual peaks at 41 and 85 cm^{-1} are assigned as the first-order scattering caused by the disorder associated with random distribution of Ag ion among the tetrahedral sites or multi-phonon processes in the perfectly ordered lattice (39). Above the transition temperature, only two broad peaks are observed at 31 and 110 cm^{-1}, which correspond to the normal zone-boundary acoustic branch and the $A_1(TO)/E_1(TO)$ mode of Ag in the tetrahedral site, respectively (40). The former mode becomes optically active due to the breakdown of selection rules induced by structural disorder.

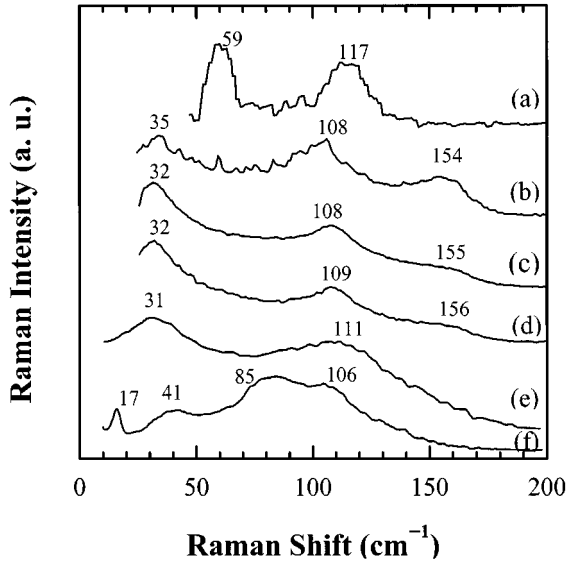

FIG. 5. Micro-Raman spectra of (a) $Bi_2Sr_2CaCu_2O_{8+\delta}$, (b) $Ag_{0.76}I_{1.17}Bi_2Sr_2CaCu_2O_{8+\delta}$, (c) $Ag_{1.00}I_{1.39}Bi_2Sr_2CaCu_2O_{8+\delta}$, (d) $Ag_{1.17}I_{1.54}Bi_2Sr_2CaCu_2O_{8+\delta}$, (e) α-AgI, and (f) β-AgI. The spectrum of α-AgI is taken from Ref. (37).

As shown in Fig. 5, there is a close similarity between the spectra of Ag–I intercalates and that of α-AgI. For all the present intercalates with different Ag and I contents, the broad peaks at ~32 and ~108 cm^{-1} are commonly observed as in α-AgI, together with the shoulder at ~155 and ~220 cm^{-1}. These peaks can be ascribed to the normal zone-boundary acoustic branch, $A_1(TO)/E_1(TO)$, $A_1(LO)/E_1(LO)$, and the overtone of $A_1(TO)/E_1(TO)$, respectively. While the first two peaks appear at the same frequencies as the counterparts of α-AgI, the $A_1(LO)/E_1(LO)$, mode has quite a higher frequency compared to that of β-AgI (124 cm^{-1}). Such an energy shift of the latter longitudinal optical mode can be reasonably understood by taking into account a significant interaction between the intercalated Ag–I layer and the host lattice along the *c* axis. It is therefore concluded that the Ag–I layer has an α-AgI-like disordered crystal structure.

From both Raman and EXAFS results, it is clarified that the interlayer Ag ion has the favorable local environment for ionic conduction, as predicted from the intercalation procedure. The ionic-conducting properties of Ag–I intercalates have been measured by impedance spectroscopy. As can be seen in Fig. 6, the silver ion conductivities of intercalates turn out to be comparable with those of the cation-substituted β-alumina compounds (41). The ionic conductivity of the Ag–I intercalate attracts special interest, since it accompanies the metallic electronic conductivity of the host block. Such a noble mixed conductor is regarded as an excellent example of multifunctional hybrid material achieved by intercalation technique.

AuI_3 Intercalate

It is well-known that the gold iodide decomposes into metal gold and molecular iodine at 100°C (28), but exhibits a quite high ionic conductivity below that temperature,

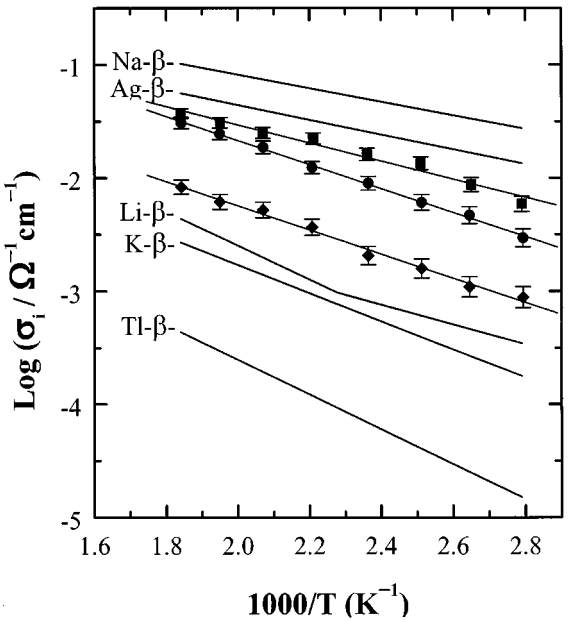

FIG. 6. Ionic conductivities of Ag–I intercalates, $Ag_{1.15}I_{1.53}Bi_2Sr_2CuO_{6+\delta}$ (solid circle), $Ag_{1.17}I_{1.54}Bi_2Sr_2CaCu_2O_{8+\delta}$ (solid square), $Ag_{1.15}I_{2.15}Bi_2Sr_2Ca_2Cu_3O_{10+\delta}$ (solid diamond), and cation substituted aluminas, M^+-β-Al_2O_3. The data for the aluminas are taken from Ref. (41).

implying that Au is remarkably mobile in the iodine matrix. Due to the excellent mobility of gold ions, the Au–I intercalate can be prepared by thermally induced Au diffusion into the preintercalated iodine layer of $IBi_2Sr_2CaCu_2O_{8+\delta}$ as demonstrated for the Ag–I intercalate. Because the preintercalated iodine is partially disintercalated during the Au ion diffusion, the composition of the finally obtained phase is determined to be $(AuI_3)_{0.25}Bi_2Sr_2CaCu_2O_{8+\delta}$.

The powder XRD patterns for the pristine $Bi_2Sr_2CaCu_2O_{8+\delta}$ and $(AuI_3)_{0.25}Bi_2Sr_2CaCu_2O_{8+\delta}$ are shown in Fig. 7. All the XRD peaks are well indexed with the tetragonal structure. The c axis lattice parameters are determined to be 30.6 Å for the pristine compound and 37.1 Å for the Au–I intercalate. Since there are two intercalant layers for each unit cell of $Bi_2Sr_2CaCu_2O_{8+\delta}$, each gold iodide layer expands the basal spacing by 3.25 Å. Such a basal increment upon Au–I intercalation is slightly smaller than that upon iodine intercalation ($\Delta d \approx 3.6$ Å), suggesting that the gold iodide forms a planar structure in between Bi_2O_2 double slabs with an enhanced chemical interaction with the host lattice, compared to the iodine intercalate. Although the gold iodide intercalation leads to an expansion of the c axis, it has little influence on the in-plane a parameter.

The temperature-dependent dc magnetic susceptibility (χ_{dc}) of the gold iodide intercalate is compared with those of the pristine compound and the iodine intercalate as shown in Fig. 8. The gold iodide intercalate exhibits a superconducting transition at 78 K, which is slightly lower than the T_c value of the pristine compound ($T_c \approx 80$ K). Such a T_c depression for the Au–I intercalate is much smaller than that for the iodine intercalate ($\Delta T_c = 10$ K), despite the similar lattice expansion of both intercalates. Such results clarify that the T_c evolution upon intercalation is closely related to the charge transfer rate (3, 17–19) rather than the modification of interblock coupling (20–22). Taking into account the minute T_c variation upon Au–I intercalation, it is reasonably expected that the intercalation of positive Au ions diminishes the hole concentration of the CuO_2 layer that is increased by iodine intercalation. In this respect, the intercalated AuI_3 species is suggested to have only a slightly negative charge probably as the form of $Au^{I}(I^{-0.33})_3$ or $Au^{III}(I^{-})_3$.

Since Au and I do not form any stable compound at the intercalation condition (235°C), it is quite interesting to investigate the chemical bonding nature and intracrystalline structure of the intercalated gold iodide. To determine local structure around the Au ion, we have performed the Au L_3-edge EXAFS analysis for the gold iodide intercalate and the reference AuI. Figure 9 represents the Fourier-filtered $k^3\chi(k)$ EXAFS spectra for both compounds and their best fits. The oscillation amplitude is found to be much larger for the Au–I intercalate than for AuI, implying that the coordination number around Au is increased upon intercalation. The nonlinear curve fitting results reveal that the interlayer Au is coordinated by three iodines with the (Au–I) bond distance of 2.56 Å, in contrast to the two-coordination ($R_{Au-I} = 2.62$ Å) in AuI. Considering the gallery height and the area demand for the Au–I layer, three-coordination of Au to I implicates the trigonal planar geometry of the AuI_3

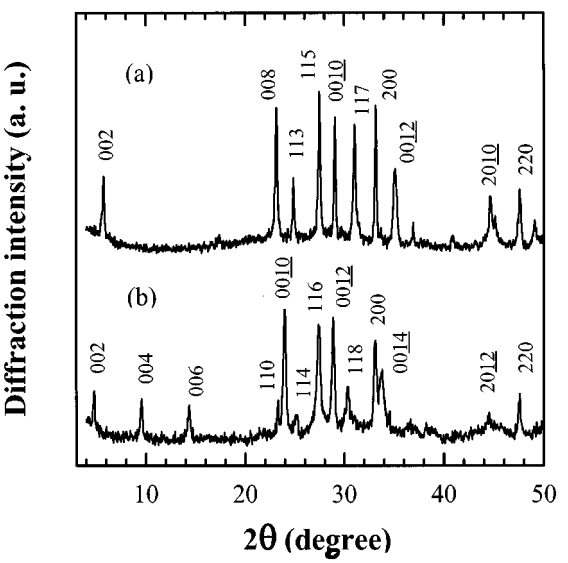

FIG. 7. Powder XRD patterns of (a) $Bi_2Sr_2CaCu_2O_{8+\delta}$ and (b) $(AuI_3)_{0.25}Bi_2Sr_2CaCu_2O_{8+\delta}$.

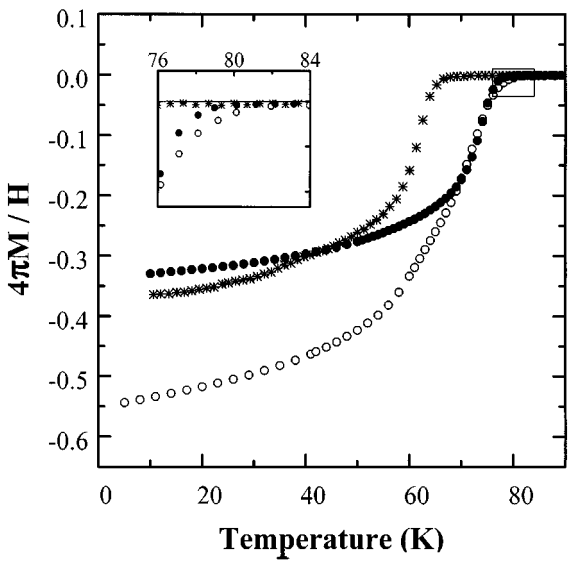

FIG. 8. The dc magnetic susceptibilities of $Bi_2Sr_2CaCu_2O_{8+\delta}$ (open circle), $IBi_2Sr_2CaCu_2O_{8+\delta}$ (asterisk), and $(AuI_3)_{0.25}Bi_2Sr_2CaCu_2O_{8+\delta}$ (solid circle). Inset shows the detailed behavior near the onset T_c for $(AuI_3)_{0.25}Bi_2Sr_2CaCu_2O_{8+\delta}$.

complex. This local structure of Au is rather exceptional; furthermore, it is also noteworthy that Au and I form a complex beyond the decomposition temperature of AuI. Such an unusual bonding character of gold iodide in $(AuI_3)_{0.25}Bi_2Sr_2CaCu_2O_{8+\delta}$ can be achieved by an effective interaction with the BiO surface in the host lattice, which is supported by the remarkable basal spacing contraction from iodine intercalate to Au–I intercalate.

CONCLUSION

We have attempted to intercalate a wide range of chemical species with various electronic and geometric structures into Bi-based cuprate superconductors, $Bi_2Sr_2Ca_{n-1}Cu_nO_{2n+4+\delta}$ ($n = 1$, 2, and 3). Among them, only soft Lewis acidic species, I_3^-, $HgBr_2^{\delta-}$, $HgI_2^{\delta-}$, $Ag_xI_w^{x-w}$, and $AuI_3^{\delta-}$ are found to form intercalation complexes with the Lewis basic host lattice. The intercalation of halogen and metal halides is revealed to be facilitated by the phase transitions from solid to liquid, vapor, and fast ion-conducting polymorphs, indicating that this reaction is governed by both thermodynamic and kinetic factors. According to the EXAFS and micro-Raman analyses, it becomes clear that the intercalated guest species maintain their high temperature forms even at room temperature. While the intercalated iodine and mercuric halide species are stabilized as linear molecules of I_3, $HgBr_2$, and HgI_2 as in vapor state, the silver iodide species are intercalated with unusual intracrystalline structures related to their superionic-conducting α-AgI phase. In the case of gold iodide intercalate, a novel AuI_3 molecular complex is identified with trigonal planar geometry, which is the first example of isolated gold iodide molecule. For all the present intercalation compounds, the regularly interstratified structures consisting of superconducting lattice and metal halide layer with various local geometries are illustrated in Fig. 10.

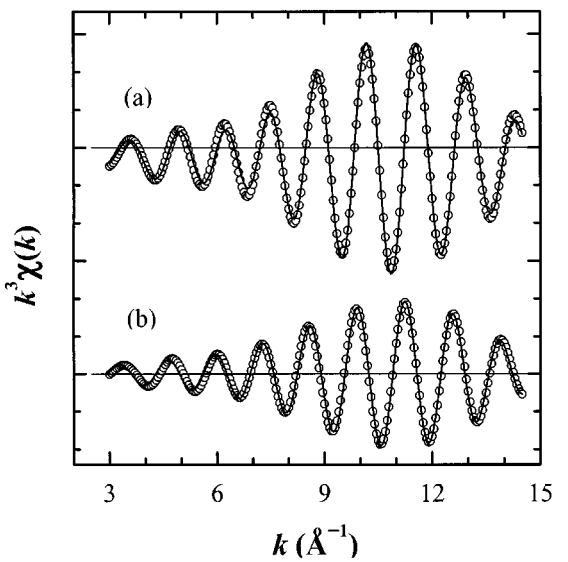

FIG. 9. Fourier-filtered Au L_3-edge EXAFS spectra for (a) $(AuI_3)_{0.25}Bi_2Sr_2CaCu_2O_{8+\delta}$ and (b) AuI (experimental, open circle; fit, solid line).

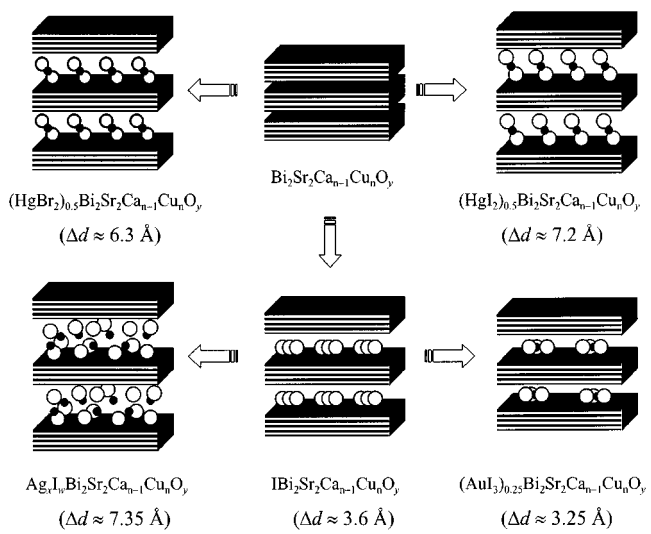

FIG. 10. Schematic illustration of the interstratified structures of iodine and metal salt intercalated $Bi_2Sr_2Ca_{n-1}Cu_nO_{2n+4+\delta}$.

ACKNOWLEDGMENTS

This work was supported by the Korea Science and Engineering Foundation (KOSEF) through the Center for Molecular Catalysis (CMC). The authors are grateful to Professor D.-K. Kim and Professor M. Kakihana for their help with the measurement of the Raman spectra.

REFERENCES

1. M. S. Dressellhaus (Ed.), "Intercalation in Layered Materials." Plenum, New York, 1986.
2. X.-D. Xiang, S. Mckernan, W. A. Vareka, A. Zettl, J. L. Corkill, T. W. Barbee III, and M. L. Cohen, *Nature* **348,** 145 (1990).
3. S.-J. Hwang, N.-G. Park, D.-H. Kim, and J.-H. Choy, *J. Solid State Chem.* **138,** 66 (1998).
4. P. V. Huong and A. L. Verma, *Phys. Rev. B* **48,** 9869 (1993).
5. G.-A. Scholtz and F.-W. Boswell, *Solid State Commun.* **74,** 959 (1990).
6. Y. Koike, T. Okubo, A. Fujiwara, T. Noji, and Y. Saito, *Solid Sate Commun.* **79,** 501 (1991).
7. J.-H. Choy, N.-G. Park, S.-J. Hwang, D.-H. Kim, and N.-H. Hur, *J. Am. Chem. Soc.* **116,** 11564 (1994).
8. J.-H. Choy, N.-G. Park, Y.-I. Kim, S.-H. Hwang, J.-S. Lee, and H.-I. Yoo, *J. Phys Chem.* **99,** 7845 (1995).
9. J.-H. Choy, N.-G. Park, Y.-I. Kim, and C.-H. Kim, *Eur. J. Solid State Inorg. Chem.* **t32,** 701 (1995).
10. H. Kumakura, J. Ye, J. Shimoyama, H. Kitaguchi, and K. Togano, *Jpn. J. Appl. Phys.* **32,** L894 (1993).
11. J.-H. Choy, N.-G. Park, S.-J. Hwang, and Z.-G. Kim, *J. Phys. Chem.* **100,** 3783 (1996).
12. J.-H. Choy, S.-J. Hwang, and N.-G. Park, *J. Am. Chem. Soc.* **119,** 1624 (1997).
13. J.-H. Choy, Y.-I. Kim, and S.-J. Hwang, *J. Phys. Chem. B.* **102,** 9191 (1998).
14. J.-H. Choy, S.-J. Hwang, and D.-K. Kim, *Phys. Rev. B* **55,** 5674 (1997).
15. J.-H. Choy, S.-J. Hwang, and S.-J. Kim, *Phys. Rev. B* **57,** 3156 (1998).
16. J.-H. Choy, S.-J. Kwon, and G.-S. Park, *Science* **280,** 1589 (1998).
17. M.-A. Subramanian, *J. Solid State Chem.* **110,** 193 (1994).
18. D. Pooke, K. Kishio, T. Kota, Y. Fukuda, N. Sandana, M. Nagoshi, K. Kitazawa, and K. Yamafuji, *Physica C* **198,** 349 (1992).
19. T. Huang, M. Itoh, J. Yu, Y. Inaguma, and T. Nakamura, *Phys. Rev. B* **49,** 9885 (1994).
20. X.-D. Xiang, A. Zettl, W. A. Vareka, J. L. Corkill, T. W. Barbee III, and M. L. Cohen, *Phys. Rev. B* **43,** 11496 (1991).
21. X.-D. Xiang, W. A. Vareka, A. Zettl, J. L. Corkill, T. W. Barbee III, M. L. Cohen, N. Kijima, and R. Gronsky, *Science* **254,** 1487 (1991).
22. J. Ma, P. Alméras, R. J. Kelley, H. Berger, G. Mararitondo, A. Umezawa, M. L. Cohen, and M. Onellion, *Physica C* **227,** 371 (1994).
23. L.-S. Grigoryan, R. Kumar, S.-K. Malik, R. Vijayaraghavan, and A. Harutymyan, *Physica C* **198,** 137 (1992).
24. J. Ricketts, R. Puzniak, C.-J. Liu, G.-D. Gu, N. Koshizuka, and Y. Yamauchi, *Appl. Phys. Lett.* **65,** 3284 (1994).
25. M. Ohashi, W. Gloffke, and M.-S. Whittingham, *Solid State Ionics* **57,** 183 (1992).
26. Y. Koike, K. Sasaki, A. Fujiwara, K. Watanabe, M. Kato, T. Noji, and Y. Saito, *Physica C* **245,** 232 (1995).
27. J. E. Huheey, E. A. Keiter, and R. L. Keiter, "Inorganic Chemistry," Harper Collins, New York, 1993.
28. J. E. Macintyre, F. M. Daniel, and V. M. Stirling, "Dictionary of Inorganic Compounds," Vol. 1, p. 125. Chapman & Hall, London, 1992.
29. A. Maeda, M. Hase, I. Tsukada, K. Noda, S. Takebayashi, and K. Uchinokura, *Phys. Rev. B* **41,** 6418 (1990).
30. C. Turbandt and E. Lorenz, *Z. Phys. B.* **87,** 513 (1913).
31. M. Teicher and R. Weil, *Phys. Rev. B* **18,** 7134 (1978).
32. A. F. Wells, "Structural Inorganic Chemistry," Clarendon, Oxford, 1984.
33. T. Yokoyama, K. Kobayashi, T. Ohta, and A. Ugawa, *Phys. Rev. B* **53,** 6111 (1996).
34. B. K. Teo, "EXAFS: Basic Principles and Data Analysis," Springer-Verlag, Berlin, 1986.
35. W. Klemperer, *J. Chem. Phys.* **25,** 1066 (1956).
36. J. Prade, A. D. Kulkarni, F. W. de Wette, U. Schröder, and W. Kress, *Phys. Rev. B* **39,** 2771 (1989).
37. G. Mariotto, A. Fontana, E. Cazzanelli, and M. P. Fontana, *Phys. Status Solidi B* **101,** 341 (1980).
38. G. L. Bottger and C. V. Damsgard, *J. Chem. Phys.* **57,** 1215 (1972).
39. B. Kh. Bairamov, N. V. Lichkova, V. D. Timofeev, and V. V. Toporov, *Sov. Phys. Solid State* **25,** 1438 (1983).
40. G. Burns, F. H. Dacol, and M. W. Shafer, *Phys. Rev. B* **16,** 1416 (1977).
41. T. Kudo and K. Fueki, "Solid State Ionics," p. 125. VCH, New York, 1990.